Colloids and Surfaces A 568 (2019) 356–361

Contents lists available at ScienceDirect

Colloids and Surfaces A

journal homepage: www.elsevier.com/locate/colsurfa

Superhydrophobic SiO_2 micro/nanofibrous membranes with porous surface prepared by freeze electrospinning for oil adsorption

Zhaowei Liu[a,b], Yufei Tang[a,b,*], Kang Zhao[a,*], Qi Zhang[a]

[a] Department of Materials Science and Engineering, Xi'an University of Technology, Xi'an 710048, PR China
[b] Key Laboratory of Corrosion and Protection of Shaanxi Province, No. 5 South Jinhua Road, Xi'an 710048, PR China

GRAPHICAL ABSTRACT

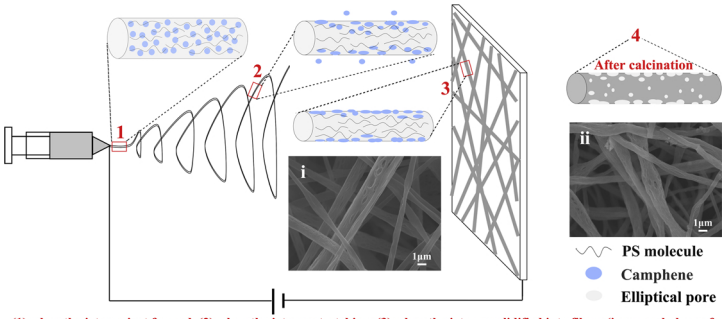

(1) when the jet was just formed, (2) when the jet was stretching, (3) when the jet was solidified into fibers (i, a morphology of composite fibers) and (4) when the fibers was calcined (ii, a morphology of porous fibers)

ARTICLE INFO

Keywords:
SiO_2 micro/nanofibrous membranes
Surface porous structure
Electrospinning
Freeze drying
Oil sorption capacity

ABSTRACT

Superhydrophobic polymer fibrous membranes have advantages in oil–water separation and oil spill treatment but are not resistant to high temperature and chemical corrosion resistance. Superhydrophobic SiO_2 micro/nanofibrous membranes are one of the research hotspots because of the high temperature stability, corrosion resistance, and low cost of SiO_2. In this study, camphene was dispersed into the SiO_2 spinning solution for freeze electrospinning. SiO_2 micro/nanofibrous membranes with porous surface were obtained by camphene sublimation through freeze drying and calcining. The effects of polystyrene and camphene contents on the surface pore structure of SiO_2 micro/nanofibrous membranes were investigated. The specific surface area of the porous fibrous membrane was approximately five times as high as that of the conventional electrospun SiO_2 micro/nanofibrous membrane. Furthermore, superhydrophobic property was obtained after hexamethyl-disilazane modification. The contact angle of porous fibrous membrane was more than 150° and the sliding angle was just 2.1°. The maximum absorption capacity of the modified SiO_2 micro/nanofibrous membrane with porous surface for three kinds of oils can reach 43.7 g/g. In addition, the absorption capacity of the porous membrane for methyl silicone oil was still higher than 34 g/g after repeated use for five times. Hence, porous SiO_2 micro/nanofibrous membranes exhibit application prospect in oil/water separation and oil pollution adsorption.

* Corresponding authors at: 5 South Jinhua Road, Xi'an, Shaanxi, 710048, PR China.
E-mail addresses: yftang@xaut.edu.cn (Y. Tang), kzhao@xaut.edu.cn (K. Zhao).

https://doi.org/10.1016/j.colsurfa.2019.02.038
Received 5 February 2019; Accepted 14 February 2019
Available online 15 February 2019

1. Introduction

Efficient oil and water separation materials and technology must be developed given the increasing industrial oily wastewater production and continuous oil leakage [1–3]. In general, materials used for oil–water separation should have hydrophobic and lipophilic properties to adsorb and separate oil from water [4,5]. In addition, oil–water separation materials should have high specific surface area to provide high oil adsorption capacity [6,7]. Therefore, nanoparticles have broad application prospects in oil–water separation due to their high specific surface area [8,9]. However, nanoparticles are not easy to recycle after use, resulting in secondary pollution [10]. Although the modified magnetic nanoparticles can be recovered [11], the low dispersion of nanoparticles in water has not been solved.

Electrospun nanofibers not only have high specific surface area [12–15] but also can easily be recycled [16]. Therefore, polymer nanofibrous membranes, such as polystyrene (PS) nanofibrous membrane [17–19] and polyacrylonitrile nanofibrous membrane [20], are widely used in oil–water separation and oil spill treatment [21–24] because of their high hydrophobicity. In addition, several scholars proposed methods for preparing polymer fibers with porous structure; the resulting materials have ultrahigh specific surface area and surface roughness and high oil absorption capacities [25–27]. However, the decomposition or softening temperature of polymer nanofibrous membrane is low, which leads to low-temperature stability when used [28,29]. In addition, fibrous membranes may be corroded by seawater or micro-organisms after prolonged use [30]. Therefore, micro/nanofibrous membranes with excellent stability must be developed. SiO_2 micro/nanofibrous membranes have been extensively used in oil–water separation [31,32], and their surface can be superhydrophobic after being modified by a hydrophobic agent. Moreover, SiO_2 fibrous membranes can be used repeatedly because of their high-temperature stability and chemical stability [33]. SiO_2 fibrous membranes prepared by electrospinning are flexible and can be easily recycled [34]. The preparation of SiO_2 micro/nanofibrous membranes with ultrahigh specific surface area is the key to obtain high oil adsorption capacity.

This paper proposes novel method that combines electrospinning and freeze drying to prepare SiO_2 micro/nanofibrous membranes with porous surface. Camphene was dispersed into the SiO_2 spinning solution for freeze electrospinning. During stretching at room temperature electrospinning, camphene was frozen, and pores were formed by frozen camphene sublimation after freeze drying. SiO_2 micro/nanofibrous membranes with porous surface were obtained after calcining. The effects of PS and camphene contents on the surface pore structure of SiO_2 micro/nanofibrous membranes were investigated. The hydrophobicity and oil adsorption capacity of the resulting micro/nanofibrous membranes were also tested. This kind of micro/nanofibrous membranes will have potential applications in oil–water separation and oil pollution adsorption treatment.

2. Experimental procedures

2.1. Fabrication of SiO_2 micro/nanofibrous membranes with porous surface

PS (Mw = ˜350,000 g/mol, Sigma Aldrich, U.S.A.) was used as the electrospun polymer. Camphene (95%, Sigma Aldrich, U.S.A.) was used as pore forming agents. Dimethylformamide (DMF, Tianjin Kemiou Chemical Reagent Co., Ltd., China) was used as the solvent. Ethyl orthosilicate (TEOS, Tianjin Kemiou Chemical Reagent Co., Ltd., China) was used as the SiO_2 precursor, and phosphoric acid (AR, Tianjin Yaohua Chemical Reagent Co., Ltd., China) was employed to promote TEOS hydrolysis. The hexamethyl-disilazane (HMDS, Tianjin Kemiou Chemical Reagent Co., Ltd., China) was utilized as a superhydrophobic modifier for SiO_2 micro/nanofibrous membranes.

PS was first mixed in 5 mL DMF of camphene (0, 1, and 2 mL) and TEOS (5 mL), followed by magnetic stirring at 40 °C for 2 h to obtain the solutions with 15, 20, and 25 wt.% PS contents. SiO_2 spinning solutions were obtained by adding the 0.25 g phosphoric acid and stirring for 24 h at room temperature. SiO_2 spinning solutions were loaded into a micropump of an electrostatic jet apparatus (KH-08, Beijing Kangsente Co., Ltd., Beijing, China). PS/SiO_2/camphene composite fibrous membranes were obtained after freeze electrospinning. Freeze electrospun parameters were as follows: spinning voltage of 24 kV, propulsion rate of 0.66 mL/h, receiving distance of 17 cm, metal receiving substrate temperature of 0 °C, and relative humidity of 70%. Finally, PS/SiO_2/camphene composite fibrous membranes were freeze dried in a freeze dryer (Freezone 2.5 L Triad; Labconco, Kansas, USA) for 12 h to remove any camphene and to obtain the porous PS/SiO_2 composite fibrous membranes. Finally, SiO_2 micro/nanofibrous membranes with porous surface were obtained after calcining for 2 h at 600 °C and cooling with the furnace. SiO_2 micro/nanofibrous membranes were placed in HMDS and soaked for 15 min and then calcined for 1 h at 190 °C for surface superhydrophobic modification. For comparison, the conventional SiO_2 micro/nanofibrous membrane, that is, no addition of camphene and the same electrospinning, was prepared.

2.2. Characterization

The infrared spectra of SiO_2 micro/nanofibrous membranes with porous surface was tested by Fourier transform infrared (FT-IR) spectroscopy (Prestige-21, Shimadzu Corporation, Tokyo, Japan) over the range of 4000–500 cm^{-1}. Morphologies of the SiO_2 micro/nanofibrous membranes after gold spraying were observed by SEM (JSM 6700, Olympus, Tokyo, Japan). Specific surface areas of the SiO_2 micro/nanofibrous membranes were characterized using a model Gemini VII 2390 analyzer. The water contact angles and sliding angles of SiO_2 micro/nanofibrous membranes were measured by JC2000 A (Shanghai Zhongchen Digital Technology Equipment Co., Shanghai, China) and DSA-100 (Kruss Company, Germany), respectively. The SiO_2 micro/nanofibrous membrane with porous surface after HMDS modification was placed in a glass beaker filled with a mixture of 30 mL oil and 20 mL water. After adsorption for 60 min, the wet membrane was drained for 60 s. The oil adsorption capacity (q, g/g) of SiO_2 micro/nanofibrous membrane with porous surface was determined by the following Eq. (1):

$$q = \frac{m_n - m}{m}, \tag{1}$$

where m_n is the total mass of the membranes after draining for 60 s, and m is the mass of the membranes before adsorption. Each sample was measured thrice to obtain the average value. The oil-adsorbed membranes were washed by industrial alcohol to remove the oil. The prepared SiO_2 micro/nanofibrous membranes were used for repeated oil absorption experiments after drying at 60 °C. Afterwards, the oil absorption capacity was calculated.

3. Results and discussion

3.1. Composition of SiO_2 micro/nanofibrous membranes with porous surface

In general, the phase of SiO_2 micro/nanofibrous membranes prepared by electrospinning is amorphous [31]. Fig. 1 shows the FT-IR spectrum of SiO_2 micro/nanofibrous membranes with porous surface. The PS raw material and the SiO_2/PS composite micro/nanofibrous membrane were also tested by FT-IR. The characteristic peaks of PS at 696.3 and 756.1 cm^{-1} were found in the PS/SiO_2 composite micro/nanofibrous membrane, that is, the C—H out of plane vibration on monosubstituted benzene ring. The characteristic peak of SiO_2 at 1109.1 cm^{-1} was also noted, indicating the Si–O–Si asymmetric vibration. In the SiO_2 micro/nanofibrous membranes with porous surface, the Si–O symmetric stretching vibrations peak at 800.5 cm^{-1} was also found. In addition, no characteristic peaks of PS indicated that PS has been completely removed after calcination.

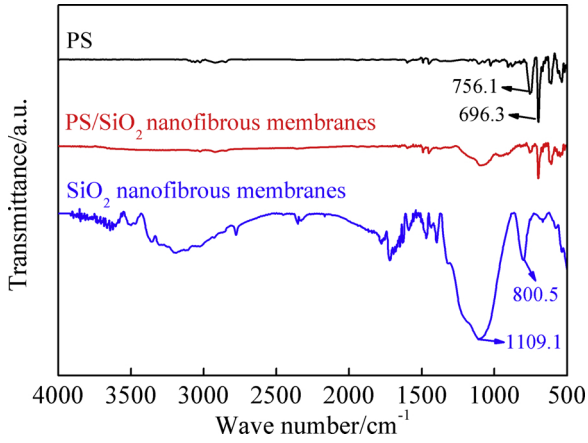

Fig. 1. FT-IR spectra of SiO_2 micro/nanofibrous membranes with porous surface.

3.2. Morphologies and porous structure of SiO_2 micro/nanofibrous membranes

Morphologies of SiO_2 micro/nanofibrous membranes with porous surface obtained by freeze electrospinning by using solutions with different PS and camphene contents are shown in Fig. 2. Fig. 2(a)–(c) show the effect of PS contents in the spinning solution on the pore structure of the SiO_2 micro/nanofibrous membrane. The camphene content was 1 ml. When the PS content was 15 wt.%, only a large number of channels was observed on the fiber surface, and no obvious pores were found. When the PS content was increased to 20 wt.%, the elliptical pores occurred on the fiber surface. However, the SiO_2 fibers were broken at 25 wt.% PS content in the spinning solution. This result indicated that the surface pore structure of the fiber in the SiO_2 micro/nanofibrous membrane was related to PS content. In addition, PS content remarkably affected the formation of pores. When the PS content was low, the viscosity of the spinning solution was low and was rapidly stretched by the electric force and gravity. The jet also was split during stretching. Camphene was elongated on the fiber surface, and the pore channel was formed. By contrast, when the PS content was high (25 wt.%), the SiO_2 fibers were loose and fractured due to the decomposition of PS during calcination.

Fig. 2(d)–(f) show morphologies of porous SiO_2 micro/nanofibrous membranes by adding different camphene contents. The PS content was 20 wt.%. Pores on the surface of SiO_2 micro/nanofibrous membrane occurred after adding camphene. With increasing camphene content, the pore number on the fiber surface also increased. The joint and adhesions was formed at the lap of micro/nanofibers because the solvent was not completely volatilized in the process of electrospinning. It is a negative impact on the specific surface area of the micro/nanofibers. The SiO_2 micro/nanofibers formed after composite fiber calcination were all bent due to the decomposition and contraction of PS in the composite fibers. When the camphene content increased to 2 mL, the SiO_2 micro/nanofibers broke remarkably. SiO_2 micro/nanofibers could not be continuous after calcination because the pores formed by camphene were too large.

To further analyze the surface pore structure of SiO_2 micro/nanofibrous membranes, a single SiO_2 micro/nanofiber was amplified and observed, as shown in Fig. 3. Fig. 3(a) shows the surface SEM morphology of the SiO_2 micro/nanofiber. A large number of irregular pores were observed on the micro/nanofiber surface, but their pore sizes were the same. This phenomenon indicated that the distribution of camphene in the spinning fluid and the jet was uniform. To explore the internal structure of porous SiO_2 micro/nanofibers, a single SiO_2 micro/nanofiber was tested by transmission electron microscopy (TEM), as shown in Fig. 3(b). In the SiO_2 micro/nanofiber, dark and light parts alternated, and the light ones were frequent. The internal density of the SiO_2 micro/nanofiber was uneven because of the porous structure in the fiber. In addition, some electron beams are easy to penetrate the pores and showed light color. Therefore, porous structures existed on the surface and inside the SiO_2 micro/nanofiber.

With the above experimental results, formation of the porous SiO_2 micro/nanofibers may be explained as the mechanism shown in Fig. 4. In electrospinning process, the high voltage electrostatic field stretched the spinning fluid into a jet. When the jet was just formed, the distribution of camphene and the PS in the jet were uniform. With the stretching of the jet, the solvent evaporated rapidly from the jet surface. The camphene began to diffuse toward the edge of the fiber. The low jet temperature reduced volatilization rate of camphene. The main purpose of high relative humidity is to reduce the volatilization rate of the camphene in the jet, so that the camphene can exist in the composite fibers. After freeze-drying,

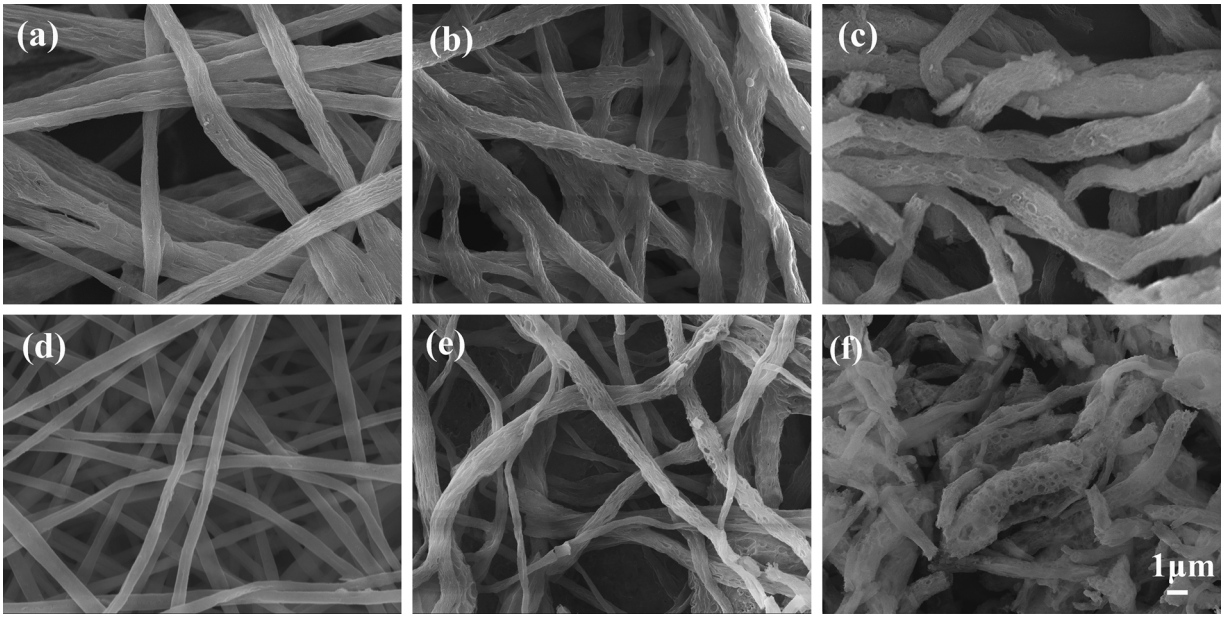

Fig. 2. Morphologies of SiO_2 micro/nanofibrous membranes with porous surface obtained by freeze electrospinning by using solutions with different PS and camphene contents: (a) 15 wt.% PS; (b) 20 wt.% PS; (c) 25 wt.% PS; (d) 0 mL camphene; (e) 1 mL camphene; and (f) 2 mL camphene.

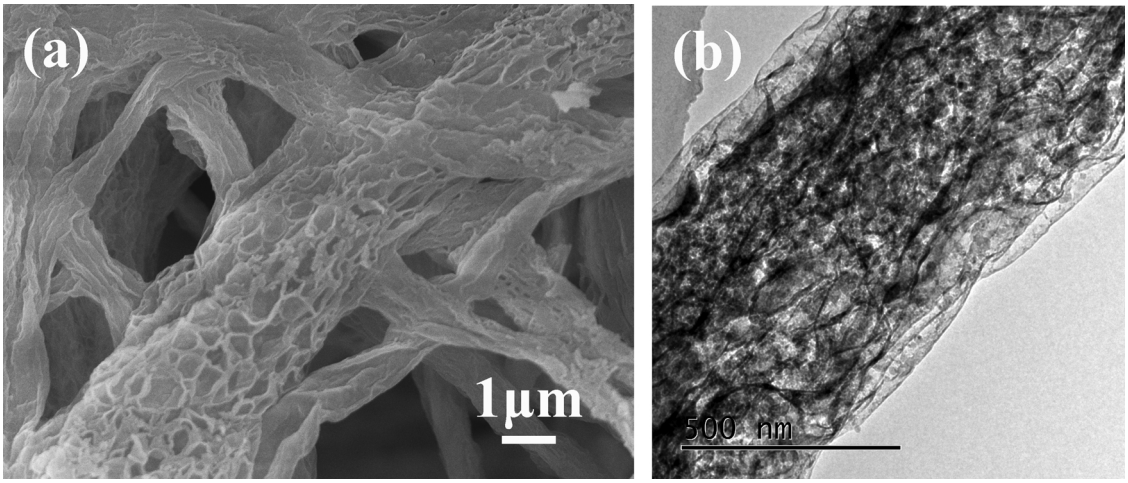

Fig. 3. Surface porous structure of SiO_2 micro/nanofibers: (a) the surface morphology (SEM); (b) the porous structure (TEM).

the camphene sublimates to form porous structure. The high relative humidity promoted the rapid solidification of PS in the jet also. Moreover, the camphene was solidified into spheres spontaneously, with the lowest spherical surface energy. However, the jet was continuously stretched. Thus, the solidified camphene finally presents the ellipse. After drying, the camphene was sublimated and pores were formed on the surface of composite micro/nanofibers. As shown in illustration (i), elliptical pores were distributed on the surface of the composite fibers. After calcined, the camphene was completely removed to form the SiO_2 micro/nanofibrous membrane with elliptical pores on the surface. The diameter of the fibers was shrunk with the decomposition of the PS. Furthermore, the decomposition of PS further had positive effects on the formation of internal pores and the enlargement of surface pores. However, the removal of PS may be lead to fiber breakage. It can be clearly observed from the illustration (ii) that elliptical pores and fiber breakage appeared on the SiO_2 micro/nanofibers.

3.3. Hydrophobicity of SiO_2 micro/nanofibrous membranes with porous surface

The porous structure on the hydrophobic fiber surface can produce high specific surface area, thereby enhancing its hydrophobic properties [35]. Fig. 5 shows Brunauer–Emmett–Teller (BET) surface curves of SiO_2 micro/nanofibrous membranes with porous surface. In Fig. 5(a), with increasing PS content, the specific surface area of the SiO_2 micro/nanofibrous membranes increased. The PS in the micro/nanofiber was decomposed and removed during the calcination, resulting in the formation of pores in the micro/nanofibers. When the PS content was 20 wt.%, the specific surface area of the SiO_2 micro/nanofibrous membrane was 106.6 m^2/g. When the PS content was 25 wt.%, the micro/nanofibers were broken after calcination and the specific surface area of the SiO_2 micro/nanofibrous membrane was the highest of 161.9 m^2/g. However, the micro/nanofibers were discontinuous, which is not conducive to practical application. The specific surface area of the SiO_2 micro/nanofibrous membrane first increased and then decreased with increasing camphene content (Fig. 5b). When the camphene content was 2 mL, a large number of SiO_2 caused serious fracture of SiO_2 micro/nanofibers, but their specific surface area decreased. It was mainly because of the joints and adhesions formed at the lap of composite micro/nanofibers. SiO_2 micro/nanofibers were agglomerated into blocks with the decomposition and shrinkage of PS after calcination.

The water droplets were absorbed by the surface of SiO_2 micro/nanofibrous membranes because SiO_2 is a hydrophilic material [36]. The contact angle of water drop on the unmodified membrane was 0°. Hydrophobic modification of SiO_2 micro/nanofibrous membrane was carried out with HMDS and the water droplets were prevented wetting. Contact

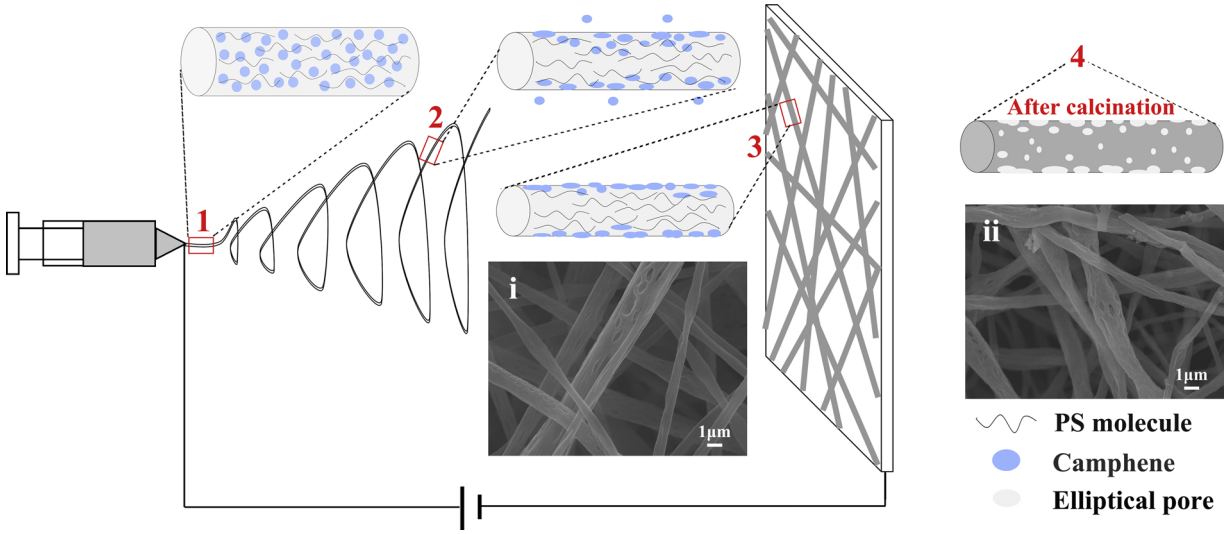

Fig. 4. Formation diagram of the porous SiO_2 micro/nanofibers: those number marks represented the states (1) when the jet was just formed, (2) when the jet was stretching, (3) when the jet was solidified into fibers (i, a morphology of composite fibers) and (4) when the fibers was calcined (ii, a morphology of porous fibers).

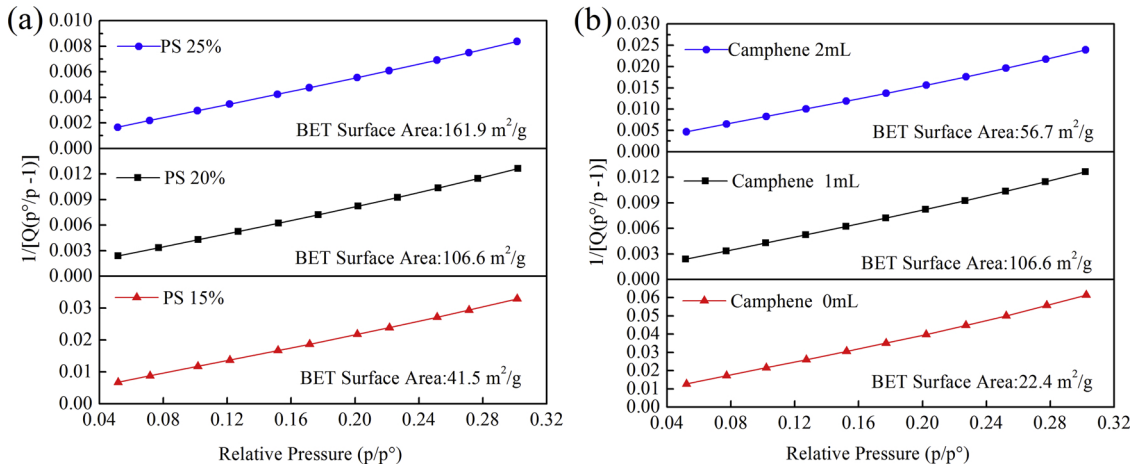

Fig. 5. BET surface curves of SiO_2 micro/nanofibrous membranes with porous surface: (a) different PS contents, the camphene content is 1 mL; (b) different camphene contents, the PS content is 20 wt.%.

angles were tested and compared with the conventional SiO_2 micro/nanofibrous membranes as shown in Fig. 6. For conventional SiO_2 micro/nanofibrous membranes (Fig. 6a), the water contact angle of water drop on the membrane was 155.49°. In the contact angle test of the SiO_2 micro/nanofibrous membrane with porous surface, the water droplet cannot drop on the surface (Fig. 6b). This result indicated that the retentive force between the droplet and the porous SiO_2 micro/nanofibrous membrane surface was small and the contact angle was more than 150°. The sliding angle of conventional SiO_2 micro/nanofibrous membranes was 16.5° while the sliding angle of porous SiO_2 micro/nanofibrous membrane was just 2.1°. This phenomenon showed that the porous SiO_2 micro/nanofibrous membrane exhibited excellent superhydrophobicity.

3.4. Oil absorption capacities of SiO_2 micro/nanofibrous membranes with porous surface

The SiO_2 micro/nanofibrous membrane with porous surface prepared by freeze electrospinning has high specific surface area and super hydrophobic property for oil. This condition can absorb oil in water to achieve the purpose of removal. Absorption capacities of SiO_2 micro/nanofibrous membranes for sunflower oil, methyl silicone oil and lubricant oil were measured, as shown in Fig. 7. Porous SiO_2 micro/nanofibrous membranes apparently showed much higher oil adsorption capacities than the conventional SiO_2 micro/nanofibrous membranes, especially for methyl silicone oil (Fig. 7a). The maximum adsorption capacity of the porous SiO_2 micro/nanofibrous membrane for methyl silicone oil was 43.7 g/g, whereas that of the conventional SiO_2 micro/nanofibrous membrane was only 18.9 g/g. From Fig. 7b, it can be clearly seen that the adsorption capacity of the porous SiO_2 micro/nanofibrous membranes gradually decreased with the increase of adsorption times and basically remained unchanged after three times adsorption. After the oil adsorption, SiO_2 micro/nanofibrous membranes with porous surface were washed by industrial alcohol, and some oil remains in the surface pores. This phenomenon decreased the oil absorption capacity. When the oil adsorption number was five times, the oil absorption of the SiO_2 micro/nanofibrous membrane with porous surface for methyl silicone oil was still larger than 34 g/g. Thus, the membrane with porous surface has a great advantage in the adsorption and removal of the oil spilled on the water.

4. Conclusions

SiO_2 micro/nanofibrous membranes with porous surface were obtained by the combination of electrospinning and freeze drying. The pores formed by camphene in the spinning solution existed on the surface of micro/nanofibers. The decomposition of PS had a positive effect on the formation of internal holes during calcination. The specific surface area of the porous fibrous membrane was approximately five times higher than that of the conventional electrospun SiO_2 micro/nanofibrous membrane. In addition, its superhydrophobic property was obtained after HMDS modification. The contact angle of porous fibrous membrane was more than 150° and the sliding angle was just 2.1°. The maximum absorption capacity of the modified SiO_2 micro/nanofibrous membrane with porous surface can reach 43.7 g/g for three kinds of oils. The absorption capacity of the resulting membrane for methyl silicone oil was still higher than 34 g/g after repeated use of five times. This condition indicated a application prospect in oil/water separation and oil pollution adsorption. However, the control of pore size and distribution on the micro/nanofiber surface needs further study in the future.

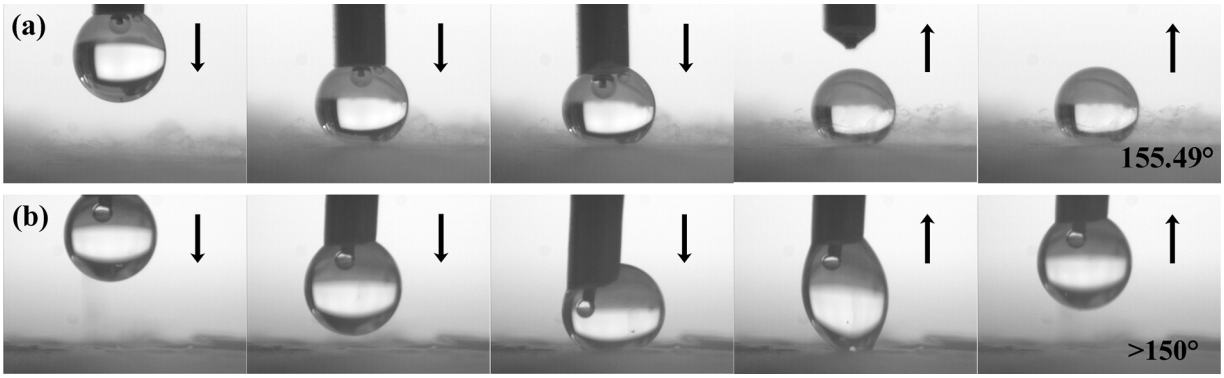

Fig. 6. Contact angle measurements of (a) conventional SiO_2 micro/nanofibrous membranes; (b) SiO_2 micro/nanofibrous membranes with porous surface by using water droplets. The arrow represents the movement direction of the droplets.

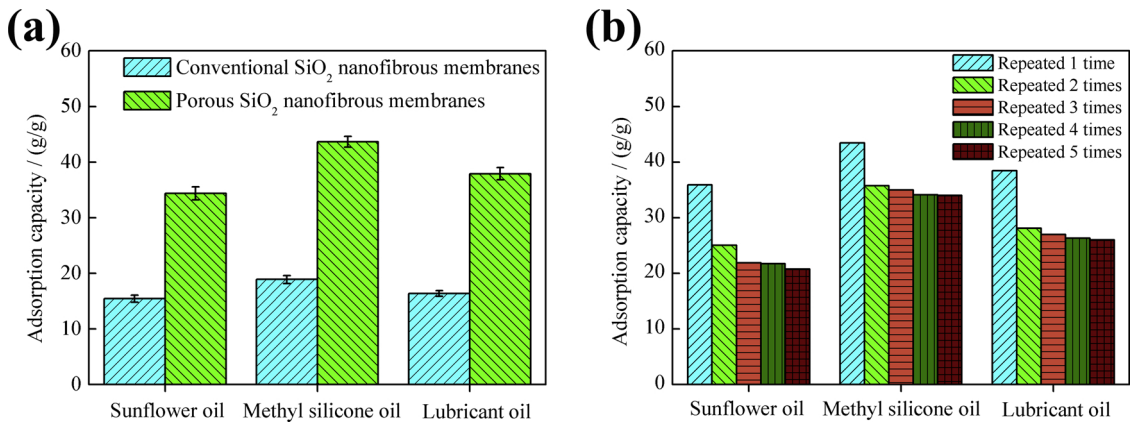

Fig. 7. (a) Absorption capacities of SiO_2 micro/nanofibrous membranes for different oils; and (b) Absorption capacities of SiO_2 micro/nanofibrous membranes with porous surface after repeated use.

Acknowledgements

The authors would like to acknowledge the support from the National Natural Science Foundation of China (Nos. 51572217 and 51672211), the China Postdoctoral Science Foundation (No. 2015M582689) and the Doctoral Innovation Fund of Xi'an University of Technology (No. 101-liuzhaowei).

References

[1] V. Singh, R.J. Kendall, K. Hake, S. Ramkumar, Crude oil sorption by raw cotton, Ind. Eng. Chem. Res. 52 (2013) 6277–6281.
[2] D. Ceylan, S. Dogu, B. Karacik, S.D. Yakan, O.S. Okay, O. Okay, Evaluation of butyl rubber as sorbent material for the removal of oil and polycyclic aromatic hydrocarbons from seawater, Environ. Sci. Technol. 43 (2009) 3846–3852.
[3] H. Zhu, S. Qiu, W. Jiang, D. Wu, C. Zhang, Evaluation of electrospun polyvinylchloride/polystyrene fibers as sorbent materials for oil spill cleanup, Environ. Sci. Technol. 45 (2011) 4527–4531.
[4] J. Wu, N. Wang, L. Wang, H. Dong, Y. Zhao, L. Jiang, Electrospun porousstructure fibrous film with high oil adsorption capacity, ACS Appl. Mater. Interfaces 4 (2012) 3207–3212.
[5] J. Lin, Y. Shang, B. Ding, J. Yang, J. Yu, S. Al-Deyab, Nanoporous polystyrenefibers for oil spill cleanup, Mar. Pollut. Bull. 64 (2012) 347–352.
[6] D. Zadaka-Amir, N. Bleiman, Y.G. Mishael, Sepiolite as an effective naturalporous adsorbent for surface oil-spill, Microporous Mesoporous Mater. 169 (2013) 153–159.
[7] M.A. Hubbe, O.J. Rojas, M. Fingas, B.S. Gupta, Cellulosic substrates for removalof pollutants from aqueous systems: a review. 3. Spilled oil and emulsifiedorganic liquids, BioResources 8 (2013) 3038–3097.
[8] G. Simonsen, M. Strand, G. Φye, Potential applications of magnetic nanoparticles within separation in the petroleum industry, J. Petrol. Sci. Eng. 165 (2018) 488–495.
[9] D. Wu, L. Fang, Y. Qin, W. Wu, H. Zhu, Oil sorbents with high sorption capacity, oil/water selectivity and reusability for oil spill cleanup, Mar. Pollut. Bull. 84 (2014) 263–267.
[10] Camilo A. Franco, Farid B. Cortés, Nashaat N. Nassar, Adsorptive removal of oil spill from oil-in-fresh water emulsions by hydrophobic alumina nanoparticles functionalized with petroleum vacuum residue, J. Colloid Interfaces Sci. 425 (2014) 168–177.
[11] Y. Chen, Y. Bai, S. Chen, J. Ju, Y. Li, T. Wang, Q. Wang, Stimuli-responsive composite particles as solid-stabilizers for effective oil harvesting, ACS Appl. Mater. Interfaces 6 (2014) 13334–13338.
[12] M. Shahhosseininia, S. Bazgir, M.D. Joupari, Fabrication and investigation of silica nanofibers via electrospinning, Mater. Sci. Eng. C 91 (2018) 502–511.
[13] C. Kuchi, G.S. Harish, P.S. Reddy, Effect of polymer concentration, needle diameter and annealing temperature on TiO_2-PVP composite nanofibers synthesized by electrospinning technique, Ceram. Int. 44 (2018) 5266–5272.
[14] D.H. Kang, H.W. Kang, Advanced electrospinning using circle electrodes for free-standing PVDF nanofiber film fabrication, Appl. Surf. Sci. 455 (2018) 251–257.
[15] N. Hernández-Navarro, V. González-González, I.E. Moreno-Cortez, M.A. Garza-Navarro, Electrospun polyvinylidene fluoride nanofibers by bubble electrospinning technique, Mater. Lett. 167 (2016) 34–37.
[16] P.K. Panda, Preparation and characterization of Samaria nanofibers by electrospinning, Ceram. Int. 39 (2013) 4523–4527.
[17] J. Gu, Z. Lv, Y. Wu, R. Zhao, L. Tian, Q. Zhang, Enhanced thermal conductivity of SiCp/PS composites by electrospinning-hot press technique, Compos. Part A-Appl. Sci. 79 (2015) 8–13.
[18] M. Zhang, J. Chen, B. Chen, J. Cao, M. Hong, C. Zhou, Q. Xu, Fabrication of polystyrene fibers with tunable co-axial hollow tubing structure for oil spill cleanup, Appl. Surf. Sci. 367 (2016) 126–133.
[19] J. Gu, Q. Zhang, J. Dang, C. Yin, S. Chen, Preparation and properties of polystyrene/SiCw/SiCp thermal conductivity composites, J. Appl. Polym. Sci. 124 (2012) 132–137.
[20] S. Samadi, S.S. Yazd, H. Abdoli, P. Jafari, M. Aliabadi, Fabrication of novel chitosan/PAN/magnetic ZSM-5 zeolite coated sponges for absorption of oil from water surfaces, Int. J. Biol. Macromol. 105 (2017) 370–376.
[21] P.P. Dorneanu, C. Cojocaru, N. Olaru, P. Samoila, A. Airinei, L. Sacarescu, Electrospun PVDF fibers and a novel PVDF/$CoFe_2O_4$ fibrous composite as nanostructured sorbent materials for oil spill cleanup, Appl. Surf. Sci. 424 (2017) 389–396.
[22] A.T. Abdulhussein, G.K. Kannarpady, A. Ghosh, B. Barnes, R.C. Steiner, P.Y. Mulon, D.E. Anderson, A.S. Biris, Facile fabrication of a free-standing superhydrophobic and superoleophilic carbon nanofiber-polymer block that effectively absorbs oils and chemical pollutants from water, Vacuum 149 (2018) 39–47.
[23] A. Almasian, M.L. Jalali, Gh. Chizari Fard, L. Maleknia, Surfactant grafted PDA-PAN nanofiber: optimization of synthesis, characterization and oil absorption property, Chem. Eng. J. 326 (2017) 1232–1241.
[24] Z. Jiang, L.D. Tijing, A. Amarjargal, C.H. Park, K.J. An, H.K. Shon, C.S. Kim, Removal of oil from water using magnetic bicomponent composite nanofibers fabricated by electrospinning, Compos. Part B-Eng. 77 (2015) 311–318.
[25] W. Liang, J. Hou, X. Fang, F. Bai, T. Zhu, F. Gao, Co Wei, X. Mo, M. Lang, Synthesis of cellulose diacetate based copolymer electrospun nanofibers for tissues scaffold, Appl. Surf. Sci. 443 (2018) 374–381.
[26] W.S. Lyoo, J.H. Youk, S.W. Lee, W.H. Park, Preparation of porous ultra-fine poly (vinyl cinnamate) fibers, Mater. Lett. 59 (2005) 3558–3562.
[27] S.K. Nataraj, K.S. Yang, T.M. Aminabhavi, Polyacrylonitrile-based nanofibers—a state-of-the-art review, Prog. Polym. Sci. 37 (2012) 487–513.
[28] J. Gu, Z. Lv, Y. Wu, Y. Guo, L. Tian, H. Qiu, W. Li, Q. Zhang, Dielectric thermally conductive boron nitride/polyimide composites with outstanding thermal stabilities via in-situ polymerization-electrospinning-hot press method, Compos. Part A-Appl. Sci. 94 (2017) 209–216.
[29] Y. Guo, G. Xu, X. Yang, K. Ruan, T. Ma, Q. Zhang, J. Gu, Y. Wu, H. Liu, Z. Guo, Significantly enhanced and precisely modeled thermal conductivity in polyimide nanocomposites with chemically modified graphene via in situ polymerization and electrospinning-hot press technology, J. Mater. Chem. C 6 (2018) 3004–3015.
[30] A. Yabuki, T. Shiraiwa, I.W. Fathona, pH-controlled self-healing polymer coatings with cellulose nanofibers providing an effective release of corrosion inhibitor, Corros. Sci. 103 (2016) 117–123.
[31] X. Wang, J. Yu, G. Sun, B. Ding, Electrospun nanofibrous materials: a versatile medium for effective oil/water separation, Mater. Today 19 (2016) 403–414.
[32] S. Ouyang, T. Wang, X. Jia, Y. Chen, J. Yao, S. Wang, Self-indicating and recyclable superhydrophobic membranes for effective oil/water separation in harsh conditions, Mater. Des. 96 (2016) 357–363.
[33] C. Wu, W. Yuan, S.S. Al-Deyab, K.Q. Zhang, Tuning porous silica nanofibers by colloid electrospinning for dye adsorption, Appl. Surf. Sci. 313 (2014) 389–395.
[34] Y. Tang, Z. Liu, S. Fu, K. Zhao, Positively charged and flexible SiO_2@ZrO_2 nanofibrous membranes and their application in adsorption and separation, RSC Adv. 8 (2018) 13018–13025.
[35] P.Y. Chen, S.H. Tung, One-step electrospinning to produce nonsolvent-induced macroporous fibers with ultrahigh oil adsorption capability, Macromolecules 50 (2017) 2528–2534.
[36] H.H. Goodarzi, M.N. Esfahany, Experimental investigation of the effects of the hydrophilic silica nanoparticles on mass transfer and hydrodynamics of single drop extraction, Sep. Purif. Technol. 170 (2016) 130–137.